2024 IEEE International Conference on Robotics and Automation (ICRA 2024)
May 13-17, 2024. Yokohama, Japan

A Planar Compliant Contact Control Applied to Multi-dimensional Elastic Gripper for Unexpected Contact

[1]Junnan Huang, [2]Xuefeng Wang, [3]Chongkun Xia, [4,*]Houde Liu, [5]Mingqi Shao, [6]Bin Liang

***Abstract*— It is difficult to guarantee an empty living environment to prevent unexpected contact between the object being manipulated by the robot and unplanned obstacles. In this paper, we propose a planar compliant contact control method for planar manipulation to cope with unexpected contact. We first use sheet gel as a multi-dimensional passive elastic element and combine it with a two-finger gripper to design a multi-dimensional elastic gripper. Subsequently, we explore the lumped parameter model for the force-displacement relationship of gel deformation and combine the model with the high impedance motion of robots to design an elastic interaction controller. The controller not only actively adjusts the deformation of the gel to provide the desired contact force and torque depending on contact, but also performs avoidance by following the surface of obstacles. Finally, we design and deploy several planar compliant contact experiments to validate the proposed method and demonstrate the unexpected contact response in human-robot co-packing. The results show that our method enables the robot to remain compliant in the face of unexpected contact caused by unplanned obstacles, which provides a guarantee for safe manipulation. Physics experiments can be viewed in the attached video.**

I. INTRODUCTION

When robots perform manipulation tasks (e.g., Human-robot collaborative manipulation [1], delivering objects [2]) in living environments, some obstacles that are not within the manipulation plan are always wandering around the motion trajectory of the manipulated object. We define the contact caused by these unplanned objects blocking the manipulated object as unexpected contact. Unlike the prepared contact such as polishing [3], tracking [4], and precision assembly [5], [6], unexpected contact is unplanned and unpredicted. Considering that unexpected contact is often accompanied by a large contact force & torque, which may lead to damage to the manipulated object or even harm the safety of humans. So compliance with unexpected contact is always an important indicator to evaluate the safety of robot manipulation. This paper takes a two-finger gripper with multi-dimensional elasticity as the manipulator and proposes a planar compliant contact control method to provide controllable compliance for the manipulated object in contact with unplanned obstacles during manipulation.

Traditional rigid robots rely on joint torque sensors [7], [8] or wrist force-torque sensors [9], [10] to guide the robot to achieve compliant contact. However, the rigid structure of robots makes it difficult to prevent transient impacts. Many researchers also try to connect passive elastic elements in series on the robot to reduce the impact [11], [12]. The force-displacement relationship of elastic elements can also be used to convert force control to position control [13], [14], which is conducive to smooth and accurate force output. Common passive elastic elements are Bowden wires [15], [16] and linear springs [17], [18], which provide elasticity in a single axis only. Some researchers attempt to achieve rotational elasticity by attaching multiple linear springs between two coaxial rings [14], [19] or by designing planar or torsion springs [20], [21]. However, these methods can only provide one-dimensional passive elasticity and are difficult to satisfy the manipulation requirements for multi-dimensional motions. Connecting multiple one-dimensional elastic elements in series can increase the dimensionality of elasticity [22], [23], but also increase the mass and complexity of structures. Excessive loading will reduce the bandwidth of front-end elastic elements, which is not conducive to accurate force output. Therefore, there is a need to find a passive elastic element that is small and has multi-dimensional elasticity.

Gel material can undergo corresponding elastic deformation when subjected to forces and torques in different dimensions, which is a kind of multi-dimensional elastomer. The elastic deformation of gel not only provides passive compliance but can also be used as a sensor to measure force or torque [24], [25]. Gelsight [26] attaches sheet gel to a rigid two-finger gripper and estimates a dense force distribution field on the gel surface by observing the gel deformation with a tiny internal camera. The small size and high elastic integration of gel make this type of gripper a great potential for multi-dimensional compliant contact. Even though there are geometric constraints on the gripping of the two-finger gripper, the gel still has a rotational and two translational degrees of freedom in the gripping plane, which can be applied to most of the planar manipulations, such as screwing a bottle cap [27], cutting fruits [28], and force-following [29]. However, current researches have focused only on using the dense force distribution field feedback of the gel to directly guide the robot manipulation while ignoring the

This work was supported by the National Key R&D Program of China(2022YFB4701400/4701402), National Natural Science Foundation of China (No. 62203260, 92248304), The Shenzhen Science Fund for Distinguished Young Scholars (RCJC20210706091946001), Guangdong Basic and Applied Basic Research Foundation (2023A1515011773), Tsinghua SIGS Cross Research and Innovation Fund (JC2021005). (Corresponding author: Houde Liu)

[1]Junnan Huang, [3]Chongkun Xia, [4,*]Houde Liu, and [5]Mingqi Shao are with the Center for Intelligent Control and Telescience, Tsinghua Shenzhen International Graduate School, Shenzhen 518055, China (e-mail: hjn21@mails.tsinghua.edu.cn; xiachongkun@sz.tsinghua.edu.cn; liu.hd@sz.tsinghua.edu.cn; smq21@mails.tsinghua.edu.cn).

[2]Xuefeng Wang is with the College of Engineering, Peking University, Beijing 100084, China (e-mail: wang_xf@pku.edu.cn).

[6]Bin Liang is with the Navigation and Control Research Center, Department of Automation, Tsinghua University, Beijing 100084, China (e-mail: bliang@tsinghua.edu.cn).

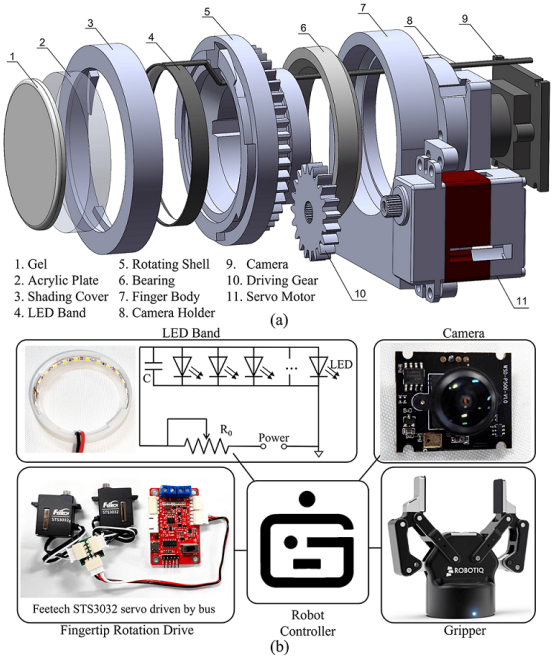

Fig. 1. Design of multi-dimensional elastic two-finger gripper. (a) The CAD exploded view of the finger. (b) The main electronic components and connections of the gripper.

passive compliance of gel as an elastic element. And the high elastic integration of gel makes its multi-dimensional elastic displacements coupled with each other, where local deformation displacements may be the superposition result of force and torque.

In this work, a planar compliant contact control method is proposed for a two-finger gripper with multi-dimensional elasticity so that the robot can more safely cope with unexpected contacts. We first explore the lumped parameter model for the force-displacement relation of gel deformation based on the contact characteristics between the gripper and the manipulated object. Then, an elastic interaction controller was designed by comprehensively considering the active damping of the robot and the passive stiffness of the gel to achieve precise and controllable multi-dimensional contact force & torque output. The controller can also guide the robot to avoid obstacles by the contact torque feedback to prevent manipulation failures. Lastly, simulations and physical experiments verify the effectiveness of our method.

II. Design of Multi-dimensional Elastic Gripper

In this section, the proposed multi-dimensional elastic gripper will be introduced. The elasticity of the gripper is mainly derived from the sheet gel on the two fingers. The components and assembly of the finger are shown in Fig. 1(a) and its electronic components are illustrated in Fig. 1(b). The width of the fingertip is 47 mm and the thickness is 34 mm. The gel is made by injecting "Hongye Q615" into a circular mold with a radius of 17 mm and a thickness of 2 mm. One side of the gel is printed with black markers and coated with a reflective membrane, while the other side is closely attached to a transparent acrylic plate fixed on the rotating shell. A camera with a resolution of 1944×2592, equipped with a wide-angle lens of 180°, is placed behind

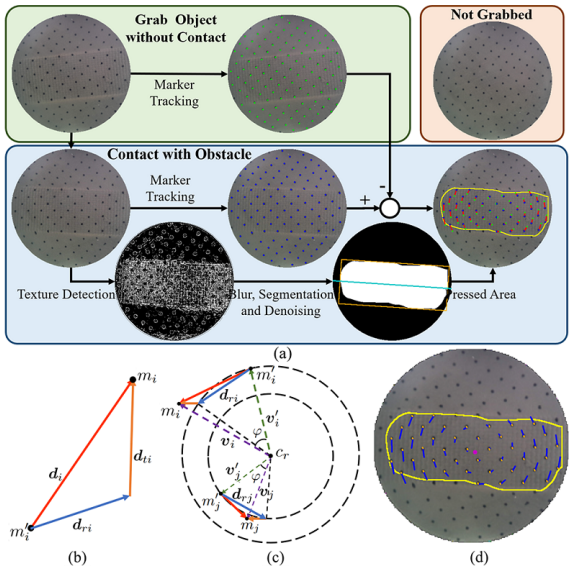

Fig. 2. Tracking and analysis of markers. (a) pressed area and markers tracking. (b) Composition of markers displacement. (c) Motion model decomposition of the markers. (d) Solving results for translational (orange) and rotational (blue) displacements, where the purple point is $\boldsymbol{c}_r$.

the acrylic plate to capture the deformation image of the gel. The LED band provides the camera with illumination inside the finger. As the manipulated object moves under external contact, the camera can capture the displacement of the markers on the surface of the gel. We also transplant the rotatable fingertips from our previous work to the gripper to improve its manipulation capability [30]. The overall fingertip, including 1-5 and 8-9 in Fig. 1(a), can be driven by a servo to rotate relative to the finger body.

III. Methodology

In this section, we propose a planar compliant contact control method applicable to the multi-dimensional elastic gripper in Sec.II. Firstly, we decouple the elastic deformation of the gel and solve the lumped parameter model for the force-displacement relationship of gel deformation. Then, we introduce an elastic interaction controller used to achieve a compliant output of contact force & torque and to guide the robot to avoid when a severe obstruction is detected.

A. Lumped parameter Model for Force-displacement Relationship of Gel Deformation

The black markers on the gel surface are displaced with elastic deformation and captured by the camera inside the finger. Tracking the markers displacement can effectively quantify the deformation of the gel, which is illustrated in Fig. 2. The gel closely fits the manipulated object under the clamping force, and the object texture is mapped onto the reflective membrane. With the help of texture detection, the pressed area in the image can be highlighted and segmented. Meanwhile, we use corner detection to obtain the location of the marker and calculate the image displacements of marks $d_i^{'}$, where i indicates that the attribute belongs to the i-th marker. Let the vertical distance from the camera focus to the pressed surface be w_c, the intrinsic matrix of the camera

be K_c, and the installation error matrix of the camera be E_m. The actual displacement d_i can be expressed as

$$\boldsymbol{d}_i = w_c \boldsymbol{E}_m \boldsymbol{K}_c \boldsymbol{d}_i^{'}. \tag{1}$$

Limited by the geometrical constraints of the two-finger gripper, the manipulated object has only two-dimensional translation and one-dimensional rotation, which correspond to the three-dimensional elasticity of the gripper. In normal work, the force between the object and the gripper does not exceed the maximum static friction, and the object is relatively stationary to the markers in the pressed area [25], which means that the motion of these markers satisfies the same Euclidean transformations (i.e., translations and rotations) as the object. As shown in Fig. 2(b), the markers displacement $\boldsymbol{d}_i$ can be regarded as a coupling of the translational displacement $\boldsymbol{d}_{ti}$ and the rotational displacement $\boldsymbol{d}_{ri}$

$$\boldsymbol{d}_i = \boldsymbol{d}_{ti} + \boldsymbol{d}_{ri}. \tag{2}$$

The translation transformation causes the object be displaced $\boldsymbol{d}_t$ in a certain direction and $\boldsymbol{d}_{ti}$ is equal for each marker, $\boldsymbol{d}_{t1} = \boldsymbol{d}_{t2} = \cdots = \boldsymbol{d}_{tN} = \boldsymbol{d}_t$. N is the number of markers in the pressed area. The rotational transformation drives markers to rotate around the center $\boldsymbol{c}_r$. Fig. 2(c) illustrates the translation and rotation of markers. Assuming that the marker moves from $\boldsymbol{m}_i'$ to $\boldsymbol{m}_i$ after contact. The vectors from $\boldsymbol{c}_r$ to $\boldsymbol{m}_i'$ and $\boldsymbol{m}_i$ are denoted by $\boldsymbol{v}_i'$ and $\boldsymbol{v}_i$. In rotational invariance, $|\boldsymbol{v}_i'| = |\boldsymbol{v}_i - \boldsymbol{d}_t|$, it can be deduced that

$$(\boldsymbol{d}_t + 2\boldsymbol{c}_r)\boldsymbol{d}_t = 2\boldsymbol{m}_i\boldsymbol{d}_t + 2\boldsymbol{d}_i\boldsymbol{c}_r - (\boldsymbol{m}_i + \boldsymbol{m}_i')\boldsymbol{d}_i. \tag{3}$$

For all markers at the same moment, $(\boldsymbol{d}_t + 2\boldsymbol{c}_r)\boldsymbol{d}_t$ is a constant. Choosing any two markers $\boldsymbol{m}_i$ and $\boldsymbol{m}_j$ in the pressed area, and (4) can be obtained.

$$\begin{aligned} &2(\boldsymbol{m}_i - \boldsymbol{m}_j)\boldsymbol{d}_t + 2(\boldsymbol{d}_i - \boldsymbol{d}_j)\boldsymbol{c}_r \\ &\quad = (\boldsymbol{m}_i + \boldsymbol{m}_i')\boldsymbol{d}_i - (\boldsymbol{m}_j + m_j')\boldsymbol{d}_j, (i \neq j) \end{aligned} \tag{4}$$

The N marks in the pressed region can form a total of $N(N-1)/2$ equations. Let $\boldsymbol{X} = [\boldsymbol{d}_t\ \boldsymbol{c}_r]^{\mathrm{T}}$, the matrix form of all equations can be described as

$$\begin{aligned} &\boldsymbol{A}\boldsymbol{X} = \boldsymbol{B}, (i \neq j), \\ &\boldsymbol{A} = \begin{bmatrix} 2(\boldsymbol{m}_1 - \boldsymbol{m}_2) & 2(\boldsymbol{d}_1 - \boldsymbol{d}_2) \\ 2(\boldsymbol{m}_1 - \boldsymbol{m}_3) & 2(\boldsymbol{d}_1 - \boldsymbol{d}_3) \\ \vdots & \vdots \\ 2(\boldsymbol{m}_{N-1} - \boldsymbol{m}_N) & 2(\boldsymbol{d}_{N-1} - \boldsymbol{d}_N) \end{bmatrix}, \\ &\boldsymbol{B} = \begin{bmatrix} (\boldsymbol{m}_1 + \boldsymbol{m}_1')\boldsymbol{d}_1 - (\boldsymbol{m}_2 + \boldsymbol{m}_2')\boldsymbol{d}_2 \\ (\boldsymbol{m}_1 + \boldsymbol{m}_1')\boldsymbol{d}_1 - (\boldsymbol{m}_3 + \boldsymbol{m}_3')\boldsymbol{d}_3 \\ \vdots \\ (\boldsymbol{m}_{N-1} + \boldsymbol{m}_{N-1}')\boldsymbol{d}_{N-1} - (\boldsymbol{m}_N + \boldsymbol{m}_N')\boldsymbol{d}_N \end{bmatrix}. \end{aligned} \tag{5}$$

$\boldsymbol{X}$ can be solved by the least squares method. The angle of the rotational transformation φ can be calculated from the vector inner product of $\boldsymbol{v}_i'$ and $(\boldsymbol{v}_i - \boldsymbol{d}_t)$

$$\varphi = arccos\left(\frac{1}{N}\sum_{i=1}^{N}\frac{\boldsymbol{v}_i' \cdot (\boldsymbol{v}_i - \boldsymbol{d}_t)}{|\boldsymbol{v}_i'|\,|\boldsymbol{v}_i - \boldsymbol{d}_t|}\right). \tag{6}$$

The elastic deformation of the gel is decoupled into a translational displacement $\boldsymbol{d}_t$ and a rotation angle φ, denoted by $\boldsymbol{q}_e = [\boldsymbol{d}_t\ \varphi]^{\mathrm{T}}$. We use (7) to map the elastic deformation to the finger force & torque $\boldsymbol{F}_e = [\boldsymbol{f}_e\ \tau_e]^{\mathrm{T}}$. The calibration of the mapping function $\boldsymbol{U}_e(x)$ is detailed in Sec.IV.A

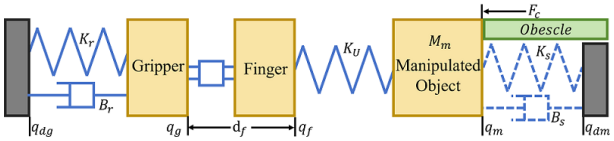

Fig. 3. Simplified single-dimensional dynamic model of the elastic gripper.

$$\boldsymbol{F}_e = \boldsymbol{U}_e(\boldsymbol{q}_e) \tag{7}$$

B. Elastic Interaction Controller

Our multi-dimensional gripper is mounted on a robot with high-impedance motion to ensure manipulation accuracy and sufficient force bandwidth, which means that the manipulated object is subjected to a combination of robot motion and gel deformation. Based on the force-displacement relationship of gel explored in Sec.III. A, we can approximate the gel as a multi-dimensional spring with stiffness matrix $\boldsymbol{K}_U$, where $\boldsymbol{K}_U$ will vary based on $\boldsymbol{U}_e$. Fig. 3 shows the simplified single-dimensional dynamic model of the elastic gripper. $\boldsymbol{B}_r$ and $\boldsymbol{K}_r$ represent the damping and stiffness matrices of the rigid robot that deploys our elastic gripper. $\boldsymbol{M}_m$ and $\boldsymbol{q}_m$ are the mass and position of the manipulated object. $\boldsymbol{q}_{dg}$ and $\boldsymbol{q}_{dm}$ are the desired positions of the gripper and the manipulated object. In the planning, the difference between $\boldsymbol{q}_{dg}$ and $\boldsymbol{q}_{dm}$ originates from the mechanical dimensions of the assembly and the initial gripping position, which is constant during the contact. In the subsequent dynamics model and control, we ignore the constant difference of $\boldsymbol{q}_{dg}$ and $\boldsymbol{q}_{dm}$ and set them as coordinate origins, $\boldsymbol{q}_{dg} = \boldsymbol{q}_{dm} = 0$. $\boldsymbol{q}_g$ and $\boldsymbol{q}_f$ denote the gripper and finger positions. $\boldsymbol{d}_f$ is the controllable motion from the gripper to fingers, where the rotational dimension relies on the servo-driven rotatable fingertip joint in Fig. 1(a), and the translational dimension will be directly superimposed on the gripper motion

$$\boldsymbol{q}_f = \boldsymbol{q}_g + \boldsymbol{d}_f. \tag{8}$$

$\boldsymbol{B}_s$ and $\boldsymbol{K}_s$ are the desired contact damping and stiffness matrices. The desired contact force $\boldsymbol{F}_{dc}$ can be described as

$$\boldsymbol{F}_{dc} = -\boldsymbol{B}_s\dot{\boldsymbol{q}}_m - \boldsymbol{K}_s\boldsymbol{q}_m \tag{9}$$

Analyzing the forces on the gripper and the manipulated object gives

$$\boldsymbol{B}_r\dot{\boldsymbol{q}}_g + \boldsymbol{K}_r\boldsymbol{q}_g + \boldsymbol{K}_U(\boldsymbol{q}_f - \boldsymbol{q}_m) = 0 \tag{10}$$

$$\boldsymbol{K}_U(\boldsymbol{q}_f - \boldsymbol{q}_m) - \boldsymbol{M}_m\ddot{\boldsymbol{q}}_m - \boldsymbol{F}_{dc} = 0 \tag{11}$$

Combining (8)-(11), the transfer functions of $\boldsymbol{q}_g$ and $\boldsymbol{q}_m$ can be obtained

$$\boldsymbol{q}_g/\boldsymbol{q}_m = \boldsymbol{Z}_1/\boldsymbol{Z}_2 \tag{12}$$

$$\boldsymbol{d}_f/\boldsymbol{q}_m = (\boldsymbol{K}_U(\boldsymbol{Z}_1 - \boldsymbol{Z}_2) - \boldsymbol{Z}_1\boldsymbol{Z}_2)/(\boldsymbol{K}_U\boldsymbol{Z}_2) \tag{13}$$

where

$$\begin{cases} \boldsymbol{Z}_1 = \boldsymbol{B}_s s + \boldsymbol{K}_s - \boldsymbol{M}_s s^2 \\ \boldsymbol{Z}_2 = \boldsymbol{B}_r s + \boldsymbol{K}_r \end{cases} \tag{14}$$

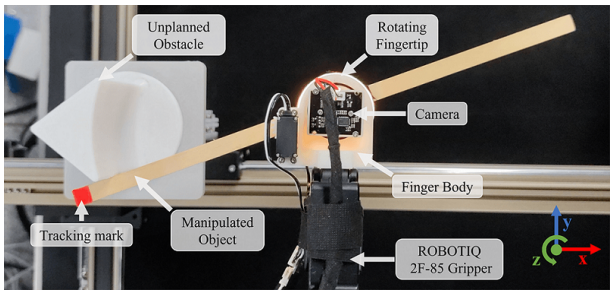

Fig. 4. Top view of the manipulated object in contact with an obstacle.

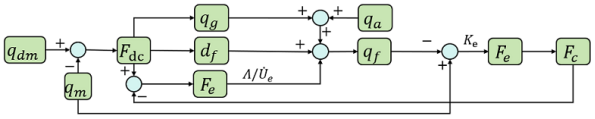

Fig. 5. The control loop of the elastic interaction controller.

In this system, $\boldsymbol{q}_g$ and $\boldsymbol{q}_f$ can be obtained from the kinematics of the robot, while $\boldsymbol{q}_m$ can be inferred from deformations of gel. The primary goal of elastic contact control is to maintain the desired contact force & torque to guarantee contact compliance. The error in contact force & torque can be expressed as

$$\boldsymbol{e}_c = \boldsymbol{F}_{dc} + \boldsymbol{M}_m \ddot{\boldsymbol{q}}_m - \boldsymbol{K}_s \boldsymbol{q}_m - \boldsymbol{K}_U(\boldsymbol{q}_g + \boldsymbol{d}_f - \boldsymbol{q}_m) + \boldsymbol{\delta} \quad (15)$$

where $\boldsymbol{\delta}$ is the uncertain mapping error, $|\boldsymbol{\delta}| \leq \boldsymbol{\delta}_{max}$. Blindly maintaining a constant impedance may cause irreversible damage to both sides of the contact if the obstacle hinders the manipulation task severely. We set a threshold F_{th} as the upper limit on the magnitude of the desired contact force & torque to prevent damage. On the elastic gripper, we adjust the deformation of the gel by controlling $\boldsymbol{d}_f$ to drive $\boldsymbol{e}_c$ to 0. The control law for $\dot{\boldsymbol{d}}_f$ is defined as

$$\begin{aligned}\dot{\boldsymbol{d}}_f = \boldsymbol{\Lambda}\boldsymbol{e}_c/\dot{\boldsymbol{U}}_e(\boldsymbol{q}_e) + \boldsymbol{\delta}\,|\boldsymbol{e}_c|/\boldsymbol{e}_c + \dot{\boldsymbol{q}}_m - \dot{\boldsymbol{q}}_g + (\boldsymbol{M}_m\ddot{\boldsymbol{q}}_m \\ -\boldsymbol{\epsilon}(|F_{th}| - |\boldsymbol{F}_{dc}|)(\boldsymbol{B}_s\dot{\boldsymbol{q}}_m + \boldsymbol{K}_s\dot{\boldsymbol{q}}_m))/\boldsymbol{K}_U\end{aligned} \quad (16)$$

where $\boldsymbol{\epsilon}(x)$ represents a step function and $\dot{\boldsymbol{U}}_e(\boldsymbol{q}_e)$ is the derivative of $\boldsymbol{U}_e(x)$ in $\boldsymbol{q}_e$. A Lyapunov function $\boldsymbol{V} = \boldsymbol{e}_c^{\mathrm{T}}\boldsymbol{e}_c/2$ is used to determine whether the contact force & torque can follow the desired value stably. The derivative of $\boldsymbol{V}$ is

$$\dot{\boldsymbol{V}} = \boldsymbol{e}_c^{\mathrm{T}}\dot{\boldsymbol{e}}_c = -\boldsymbol{\Lambda}\boldsymbol{K}_U/\dot{\boldsymbol{U}}_e(\boldsymbol{q}_e)\boldsymbol{e}_c^{\mathrm{T}}\boldsymbol{e}_c - \boldsymbol{\delta}\,|\boldsymbol{e}_c| \quad (17)$$

Since the force-displacement relationship of gel deformation is positively correlated, $\dot{\boldsymbol{U}}_e(\boldsymbol{q}_e) > 0$ and $\dot{\boldsymbol{V}} < 0$ are constant. The system can stabilize.

Fig.4 shows a top view of unexpected contact, where the obstacle tends to cause the manipulated object to turn to one side. In addition to maintaining the compliance of contact, we also try to prevent manipulation failure by guiding the robot to avoid obstacles. An active avoidance velocity $\boldsymbol{v}_a$ is introduced to $\boldsymbol{q}_g$ if the magnitude of $\boldsymbol{F}_{dc}$ exceeds $\boldsymbol{F}_{th}$. To reduce the conflict between $\boldsymbol{v}_a$ and manipulation goal, $\boldsymbol{v}_a$ is orthogonal to the desired velocity of the gripper $\boldsymbol{v}_{dg}$. Meanwhile, the magnitude of $\boldsymbol{v}_a$ is positively correlated with the contact torque τ_c and $\boldsymbol{v}_{dg}$ to prevent the sudden approach of obstacles. $\boldsymbol{v}_a$ can be described as

$$\boldsymbol{v}_a = \lambda\tau_c\boldsymbol{R}_c\boldsymbol{v}_{dg}\boldsymbol{\epsilon}(|F_{th}| - |\boldsymbol{F}_{dc}|) \quad (18)$$

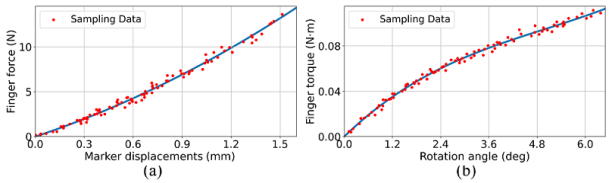

Fig. 6. The sampling data and mapping function of the calibration experiment. (a) Finger force. (b) Finger torque.

where λ is the gain parameter of the avoidance velocity and $\boldsymbol{R}_c$ is the rotation matrix of the clockwise rotation vector by 90 degrees. Combining contact compliance and obstacle avoidance, the control loop of the elastic interaction controller is demonstrated in Fig. 5.

IV. Experiments and Discussion

In this section, the mapping function in (7) is calibrated first. Subsequently, the feasibility of planar compliant contact control is tested in simulation. Finally, we deploy the multi-dimensional elastic gripper on the UR Robot and demonstrate the proposed method in the face of unexpected contact in the physical environment with static and dynamic obstacles.

A. Calibration of Force-displacement Relationship of Gel Deformation

The two fingers are disassembled during the calibration process. One of the fingers is mounted on the end of the UR Robot equipped with a wrist F/T sensor (ATI F/T Gamma), which is used to measure the ground truth of finger force & torque. And the other finger is fixed to the calibration platform. The UR Robot is controlled to drive two fingers to grasp a manipulated object as if they are mounted on the gripper. An external pusher is used to make contact with the object to induce the deformation of the fingertip gel. The displacements & rotation angles of the markers and the wrist F/T sensor measurements are recorded during contact, where the translational displacement and force take their magnitude as the recorded values. After several random contacts, Fig. 6 can be plotted, where the mapping function for finger force $\boldsymbol{U}_{ef}$ is fitted as a quadratic curve and for finger torque $U_{e\tau}$ is a cubic curve. The parameters of the two curves are shown in Table I. The sampled data is densely distributed around the calibration curve, and it can be assumed that the calibrated $\boldsymbol{U}_{ef}$ and $U_{e\tau}$ have good mapping ability. The RMSE of finger force & torque calibration are 0.3549 N & 0.002342 N·m, which can be considered as the upper limit of the uncertain mapping err in (15).

TABLE I
Mapping Function Parameter

Type	Function Expression	k_3	k_2	k_1
Contact Force	$y = k_2x^2 + k_1x$	0	9.59e-4	1.37e-1
Contact Torque	$y = k_3x^3 + k_2x^2 + k_1x$	3.07e-4	-4.60e-3	3.43e-2

B. Simulation and Analysis

In the simulation, the manipulated object is abstracted as a batten without width. If unexpected contact occurs, the object is considered to be pushed based on mechanical interference constraints, and the gel is deformed accordingly.

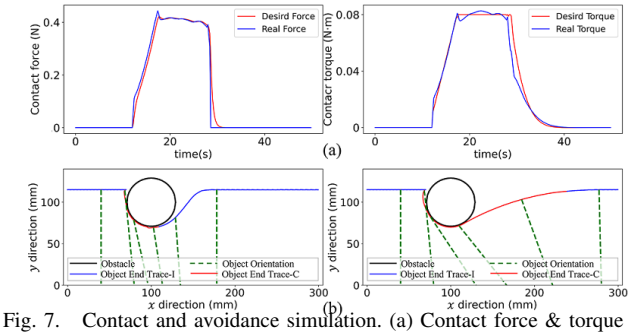

Fig. 7. Contact and avoidance simulation. (a) Contact force & torque (b) The top view of the contact scenario in the simulation, with avoidance on the left and no avoidance on the right. Blue indicates that the expected contact torque is less than the preset threshold, and red indicates the opposite.

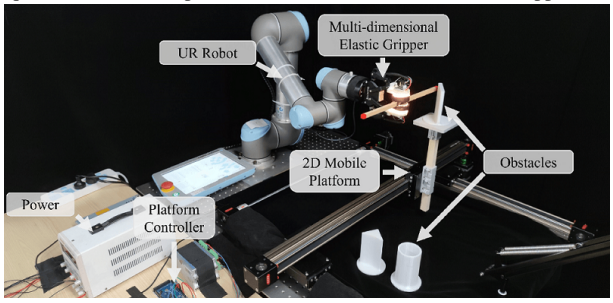

Fig. 8. The physical experiment environment.

The contact force & torque thresholds are set to 2 N & 0.08 N·m. We select a cylindrical obstacle and randomly place it near the motion path of the manipulated object. The robot is unaware of the existence of the obstacle and makes unexpected contact with it. The contact force & torque are recorded and plotted in Fig. 7(a). It can be found that the contact acts mainly on the torque. The contact force is well below the threshold, and the contact torque is stabilized in the safe range after exceeding the threshold. To demonstrate the need for active avoidance, experiments without avoidance are also performed for comparison. The simulation results for avoidance and non-avoidance are plotted in the left and right columns of Fig. 7(b), respectively. In the avoidance experiment, as the contact torque exceeds the preset threshold, the obstacle is considered to be a serious hindrance for manipulation and active avoidance is triggered. The object first gradually moves away from the obstacle and slides along the surface of the obstacle. After leaving the obstacle, the object resumes its original trajectory. From Fig. 7(b), we can find that active avoidance can greatly reduce the range and amplitude of the object affected by the obstacle.

C. Physical Experiment

In physical experiments, our elastic gripper is deployed on a UR robot and a 0.2s control cycle to validate the effectiveness of the planar compliant contact control on the physical environment, as shown in Fig. 8. Static standard obstacles and dynamic daily obstacles are employed to trigger different unexpected contacts. In addition, we demonstrate a practical application in human-robot co-packaging.

1) Static Standard Obstacles: This experiment focused on exploring whether the physical multi-dimensional elastic gripper can cope with unexpected contact as well as simulations. The common obstacle surface is composed of a mixture of three elements: concave, convex and plane. Three standard obstacles are 3D printed based on the three elements and placed on a controllable 2D mobile platform, as shown in the first column of Fig. 9. The platform will deploy these obstacles randomly around the trajectory of the object and remain stationary. We chose a $10\times10\times500$ mm batten with a red tracking marker at the end to simulate a long object that tends to contact obstacles, as shown in Fig. 4. The performance of the robot in the face of static standard obstacles is presented in Fig. 9, where the four columns from left to right are the static standard obstacles, the simplified top view, the contact torque, and the position of object & gripper. The object slides along the surface of the obstacle under the control of the gripper and successfully bypasses the obstacle that hinders manipulation. There is a fluctuation in the end trajectory of the batten just as it passes over the obstacle. The main reason for the fluctuation is that the contraction rate of the gel is not linear, but is a fast and then slow process, and does not affect the compliant contact of the object with the obstacle. From the third and fourth columns of Fig. 9, it can be found that our gripper can adjust the fingertip joint based on the contact torque to achieve a proper torque output. Limited by the fingertip servo, step vibration may occur at low-speed motion and can be mitigated if a motor with a high reduction ratio is used.

TABLE II
FOUR DAILY OBSTACLES

Obstacle	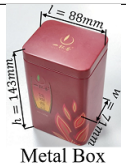 Metal Box	 Teacup	 Wine Bottle	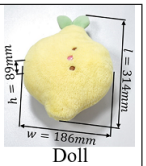 Doll
Transparency	Low	High	Middle	Low
Stiffness	High	High	High	Middle
Roughness	Low	Low	Low	Middle

2) Dynamic Daily Obstacles: Dynamic obstacles have greater unpredictability than static obstacles. Even if the robot abandons the manipulation and remains stationary, dynamic obstacles may actively approach the manipulated object and cause safety accidents. To conform to the real scene, we added trays to the ends of the batten and placed glasses filled with water to mimic the serving robot delivering objects, as shown in Fig. 10(a). We select the four representative daily obstacles (i.e. metal box, teacup, wine bottle and doll) to recreate different contacts. The detailed attributes of the four obstacles are listed in Table II. The metal box represents the generally visible rigid obstacle; the teacup represents a transparent obstacle that is difficult to detect by vision; the wine bottle represents a fragile obstacle with a high center of gravity; and the doll represents a flexible obstacle that can be deformed. The four obstacles will wander around the target trajectory of the tray driven by the 2D mobile platform. In this experiment, the tray held by the UR robot successfully bypasses the active approach obstacle and does not spill the water from the glasses, demonstrating good robustness to different stiffness and surface roughness. Our approach does not rely on external vision and is not

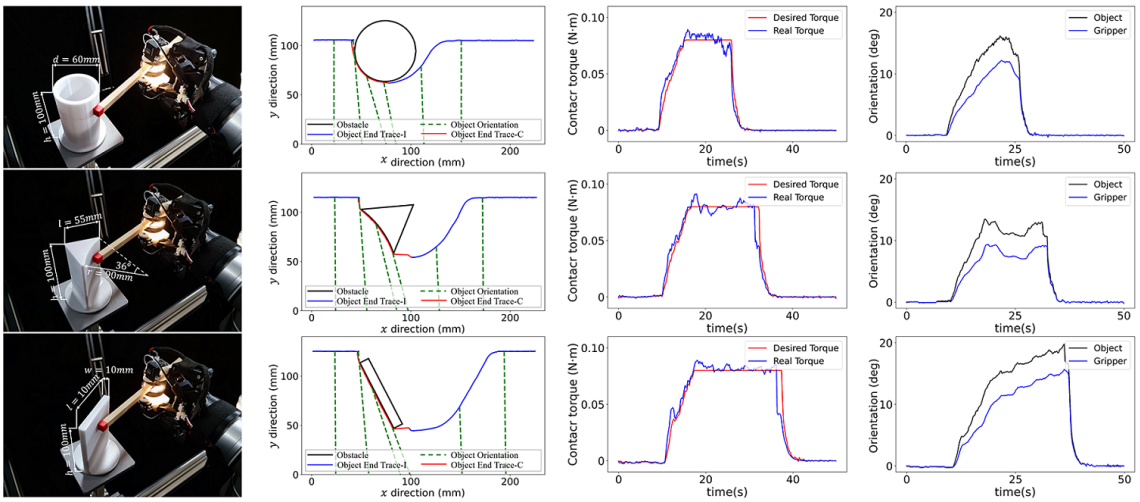

Fig. 9. The results of physical experiments. The first column is the obstacle type, the second column is the top view trajectories of the batten end that is tracked by the external camera, the third column is the contact torque, and the fourth column is the orientation angle of the batten and gripper.

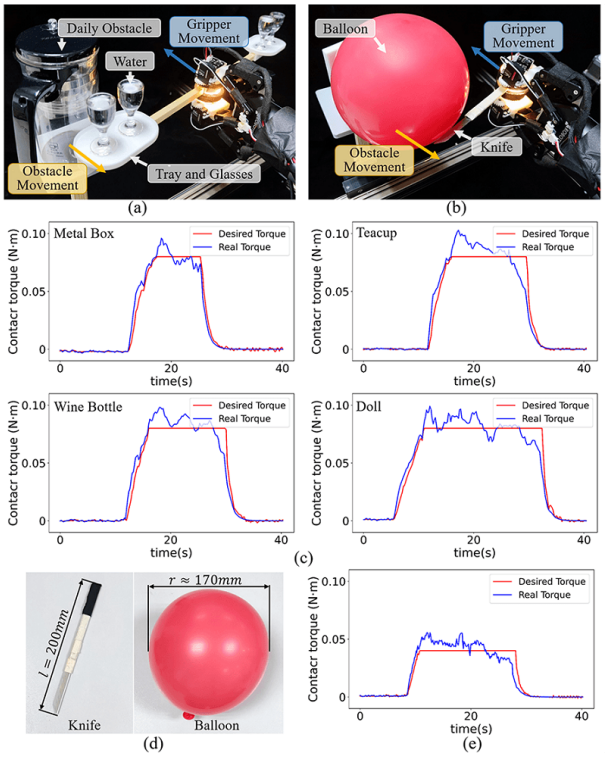

Fig. 10. Unexpected contact experiments with dynamic daily obstacles. (a) Contact occurs during the robot hands tray to deliver water. (b) The knife held by the robot unexpectedly contacts a balloon. (c) The contact torque in the dynamic daily obstacle experiments. (d) Knife and balloon in the experiments. (e) The contact torque during knife-balloon contact.

afraid of transparent objects, which troubles traditional vision solutions. Fig. 10(c) plots the contact torque during the contact between the tray and the dynamic obstacles. In addition, we allow the robot holding the knife to make unexpected contact with the balloon simulating human skin after adjusting The threshold of contact torque to verify the safety of human-robot collaborative manipulation, as shown in Fig. 10(b). Fig. 10(d) shows the size of the knife and balloon. The contact torque during the knife cutting across the balloon is illustrated in Fig. 10(e), from which high-frequency fluctuations can be observed. The fluctuations can be attributed to two factors: on the one hand, the balloon is so

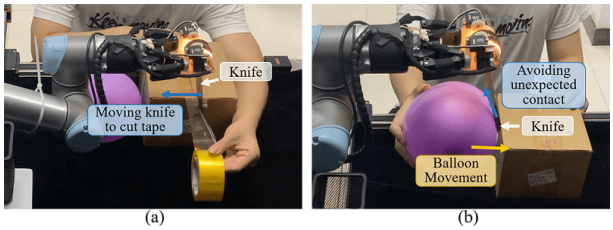

Fig. 11. Human-robot co-packaging. (a) Cutting tape as the planned contact. (b) Cutting balloons as the unexpected contact.

light that the vibrations caused by the motion of the moving platform are amplified on the balloon; on the other hand, the surface of the balloon is relatively rough, and the friction caused by contact can also cause vibration. To demonstrate the distinction between planned and unexpected contact in robot handling, we construct a human-robot co-packaging scenario, where the tape cut is set to a planned contact and the contact with the balloon is unexpected. We can observe that the knife safely slid over the surface of the balloon after cutting the tape, as shown in Fig. 11. Human safety is guaranteed in this manipulation. All the physical experiments and contact processes can be viewed in the attached video.

V. Conclusion

This paper considers unexpected contact between a manipulated object and an unplanned obstacle in the living environment and proposes a planar compliant contact control method applied to a multi-dimensional elastic gripper. The method focuses on analyzing and controlling the elastic deformation of the gripping fingertip gel to maintain proper contact force & torque and guide the robot to avoid obstacles during contact safely. Simulations and physical experiments demonstrate that the planar compliant control method is effective in guaranteeing compliance and safety of contact, whether the unexpected contact is caused by static or dynamic obstacles. Limited by the two-finger gripper constraints, our method only ensures the elasticity in-plane. Future work will consider 6D elastic applications of gel in multi-finger grippers.

REFERENCES

[1] M. L. Elwin, B. Strong, R. A. Freeman, and K. M. Lynch, "Human-multirobot collaborative mobile manipulation: The omnid mocobots," *IEEE Robotics and Automation Letters*, vol. 8, no. 1, pp. 376–383, Jan 2023.

[2] A. Edsinger and C. C. Kemp, "Human-robot interaction for cooperative manipulation: Handing objects to one another," in *RO-MAN 2007 - The 16th IEEE International Symposium on Robot and Human Interactive Communication*, Aug 2007, pp. 1167–1172.

[3] F. Lin and T. Lü, "Development of a robot system for complex surfaces polishing based on cl data," *The International Journal of Advanced Manufacturing Technology*, vol. 26, no. 9-10, pp. 1132–1137, Apr 2004.

[4] Z. Xie and Z. Yan, "Varying rate adaptive hybrid position–impedance control for robot-assisted ultrasonic examination system," *Mechanical Sciences*, vol. 13, no. 1, pp. 559–575, Apr 2022.

[5] D. Xing, X. Liu, F. Liu, and D. Xu, "Efficient insertion strategy for precision assembly with uncertainties using a passive mechanism," *IEEE Transactions on Industrial Informatics*, vol. 17, no. 2, pp. 1263–1273, Feb 2021.

[6] Y. Gai, J. Guo, D. Wu, and K. Chen, "Feature-based compliance control for precise peg-in-hole assembly," *IEEE Transactions on Industrial Electronics*, vol. 69, no. 9, pp. 9309–9319, Sep 2022.

[7] Y. Yamada, Y. Hirasawa, S. Huang, Y. Umetani, and K. Suita, "Human-robot contact in the safeguarding space," *IEEE/ASME Transactions on Mechatronics*, vol. 2, no. 4, pp. 230–236, Dec 1997.

[8] M. Jorda, E. G. Herrero, and O. Khatib, "Contact-driven posture behavior for safe and interactive robot operation," in *2019 International Conference on Robotics and Automation (ICRA)*, May 2019, pp. 9243–9249.

[9] S. Lu, J. Chung, and S. Velinsky, "Human-robot collision detection and identification based on wrist and base force/torque sensors," in *Proceedings of the 2005 IEEE International Conference on Robotics and Automation*, Apr 2005, pp. 3796–3801.

[10] K. Bai, W. Chen, K.-M. Lee, Z. Que, and R. Huang, "Spherical wrist with hybrid motion-impedance control for enhanced robotic manipulations," *IEEE Transactions on Robotics*, vol. 38, no. 2, pp. 1174–1185, Apr 2022.

[11] H. Woo, B. Na, and K. Kong, "Design of a compact rotary series elastic actuator for improved actuation transparency and mechanical safety," in *2017 IEEE International Conference on Robotics and Automation (ICRA)*, May 2017, pp. 1872–1877.

[12] G. Pratt and M. Williamson, "Series elastic actuators," in *Proceedings 1995 IEEE/RSJ International Conference on Intelligent Robots and Systems. Human Robot Interaction and Cooperative Robots*, vol. 1, Aug 1995, pp. 399–406.

[13] L. H. Blumenschein, C. G. McDonald, and M. K. O'Malley, "A cable-based series elastic actuator with conduit sensor for wearable exoskeletons," in *2017 IEEE International Conference on Robotics and Automation (ICRA)*, May 2017, pp. 6687–6693.

[14] Y. Qian, S. Han, G. Aguirre-Ollinger, C. Fu, and H. Yu, "Design, modeling, and control of a reconfigurable rotary series elastic actuator with nonlinear stiffness for assistive robots," *Mechatronics*, vol. 86, p. 102872, Oct 2022.

[15] G. Aguirre-Ollinger and H. Yu, "Lower-limb exoskeleton with variable-structure series elastic actuators: Phase-synchronized force control for gait asymmetry correction," *IEEE Transactions on Robotics*, vol. 37, no. 3, pp. 763–779, 2020.

[16] A. Erwin, N. Moser, C. G. McDonald, and M. K. O'Malley, "A bowden cable-based series elastic actuation module for assessing the human wrist," in *Dynamic Systems and Control Conference*, vol. 51890, Nov 2018, pp. 8963–8370.

[17] C.-Y. Chen, J. Dai, G. Yang, C. Wang, Y. Li, and L. Chen, "Sensor-based force decouple controller design of macro–mini manipulator," *Robotics and Computer-Integrated Manufacturing*, vol. 79, p. 102415, Feb 2023.

[18] D. Robinson, J. Pratt, D. Paluska, and G. Pratt, "Series elastic actuator development for a biomimetic walking robot," in *1999 IEEE/ASME International Conference on Advanced Intelligent Mechatronics (Cat. No.99TH8399)*, Sep 1999, pp. 561–568.

[19] T. Chen, R. Casas, and P. S. Lum, "An elbow exoskeleton for upper limb rehabilitation with series elastic actuator and cable-driven differential," *IEEE Transactions on Robotics*, vol. 35, no. 6, pp. 1464–1474, Aug 2019.

[20] N. Georgiev and J. Burdick, "Optimization-based design and analysis of planar rotary springs," in *2018 IEEE/RSJ International Conference on Intelligent Robots and Systems (IROS)*, Oct 2018, pp. 927–934.

[21] B. DeBoon, S. Nokleby, N. La Delfa, and C. Rossa, "Differentially-clutched series elastic actuator for robot-aided musculoskeletal rehabilitation," in *2019 International Conference on Robotics and Automation (ICRA)*, May 2019, pp. 1507–1513.

[22] R. C. Luo, Y. H. Pu, C. H. Chen, J. R. Chang, and C. Y. Li, "Design and implementation of humanoid biped walking robot mechanism towards natural walking," in *2011 IEEE International Conference on Robotics and Biomimetics*, Apr 2011, pp. 1165–1170.

[23] M. Bolignari, A. Mo, M. Fontana, and A. Badri-Spröwitz, "Diaphragm ankle actuation for efficient series elastic legged robot hopping," in *2022 IEEE/RSJ International Conference on Intelligent Robots and Systems (IROS)*, Oct 2022, pp. 4279–4286.

[24] C. Sferrazza, A. Wahlsten, C. Trueeb, and R. D'Andrea, "Ground truth force distribution for learning-based tactile sensing: A finite element approach," *IEEE Access*, vol. 7, pp. 173 438–173 449, Nov 2019.

[25] R. Kolamuri, Z. Si, Y. Zhang, A. Agarwal, and W. Yuan, "Improving grasp stability with rotation measurement from tactile sensing," in *2021 IEEE/RSJ International Conference on Intelligent Robots and Systems (IROS)*, Sep 2021, pp. 6809–6816.

[26] W. Yuan, S. Dong, and E. H. Adelson, "Gelsight: High-resolution robot tactile sensors for estimating geometry and force," *Sensors*, vol. 17, no. 12, p. 2762, Nov 2017.

[27] S. Dong, D. Ma, E. Donlon, and A. Rodriguez, "Maintaining grasps within slipping bounds by monitoring incipient slip," in *2019 International Conference on Robotics and Automation (ICRA)*, May 2019, pp. 3818–3824.

[28] A. Yamaguchi and C. G. Atkeson, "Combining finger vision and optical tactile sensing: Reducing and handling errors while cutting vegetables," in *2016 IEEE-RAS 16th International Conference on Humanoid Robots (Humanoids)*, Nov 2016, pp. 1045–1051.

[29] W. Kim, W. D. Kim, J.-J. Kim, C.-H. Kim, and J. Kim, "Uvtac: Switchable uv marker-based tactile sensing finger for effective force estimation and object localization," *IEEE Robotics and Automation Letters*, vol. 7, no. 3, pp. 6036–6043, Mar 2022.

[30] W. Zhang, C. Xia, X. Zhu, H. Liu, and B. Liang, "Tacrot: A parallel-jaw gripper with rotatable tactile sensors for in-hand manipulation," in *2022 IEEE International Conference on Systems, Man, and Cybernetics (SMC)*, Oct 2022, pp. 423–429.